Optical and Quantum Electronics (2024) 56:1098
https://doi.org/10.1007/s11082-024-06809-6

Effect of titanium ion doping on γ-ray shielding, structure and dielectric characteristics of glasses made of barium zinc borate

Norah A. M. Alsaif[1] · Adel M. El-Refaey[2] · R. A. Elsad[3] · M. S. Shams[2,4] · W. M. Almutairi[1] · Y. S. Rammah[5]

Received: 12 January 2024 / Accepted: 7 March 2024 / Published online: 20 May 2024

Abstract
An investigation was conducted into the impact of titanium ion (TiO_2) on the structural, dielectric, and shielding characteristics of glasses. Density improved from 3.70 to 3.93 g cm^{-3} as samples containing titanium ions rose from 0.0 to 10 mol% in the glasses network. FTIR investigations revealed the development of functional groups and units, including bridging BO_4 and non-bridging BO_3, in our recently developed glasses. Throughout the low frequency range, the dielectric constant of every glass filled with various amounts of TiO_2 mol% sharply decreased as frequency increased. The dielectric constant value appeared semi-constant as the TiO_2 level increased to 4 mol% and then increased at higher concentrations. Every glass that was examined showed distinct relaxation peaks on their measured loss tangent (tan δ) between 100 Hz and 20 kHz. The exposure (EBF) as well as energy absorption (EABF) buildup factors of Ti-X glasses were computed using Phy-X/PSD software as a function of photon energy at 1–40 MFP. Both EBF and EABF improved with increasing photon energy until they reached a maximum, at which point they declined as photon energy continued to rise. The Ti-10.0 glass sample which contains the highest doping of the TiO_2 is the most effective removal cross-section. The sample Ti-10.0 had the lowest relaxation length (λ_{FCS}) and half value layer (HVL_{FCS}).

Keywords Tan δ · Half value layer · Dielectric constant · Bridging units · Half value layer · Building factors

✉ R. A. Elsad
ragab.elsad@gmail.com

[1] Department of Physics, College of Science, Princess Nourah Bint Abdulrahman University, P.O. Box 84428, 11671 Riyadh, Saudi Arabia

[2] Department of Basic and Applied Science, Collage of Engineering and Technology, Arab Academy of Science, Technology and Maritime Transport, Smart Village, Giza, Egypt

[3] Basic Engineering Science Department, Faculty of Engineering, Menoufia University, Shebin El-Koom 32511, Egypt

[4] Physics and Mathematical Engineering Department, Faculty of Electronic Engineering, Menoufia University, Menouf 32952, Egypt

[5] Department of Physics, Faculty of Science, Menoufia University, Shebin El-Koom 32511, Egypt

1 Introduction

Glass is a category of material that is utilized in many different applications because it combines optical clarity, ease of molding, and low cost. Borate glasses are a good option for fiberglass applications because of their unique qualities, among them higher toughness, greater dielectric qualities, thermal endurance (especially during elevated temperatures), and durability against thermal expansion (Khattari et al. 2022a, 2022b; Rammah et al. 2022, 2020; Alsaif et al. 2022a, 2023a 2023b; Alrowaili et al. 2023; Zakaly 2021). The boroxol ring B_3O_6 is the boron atoms' prevalent glass structure in pure B_2O_3. A modifier is added to pure B_2O_3 to break the boroxol ring B_3O_6, resulting in BO_3 and BO_4 units (Lakshminarayana et al. 2018; Kaky et al. 2019). Depending on the type and quantity of added modifier, BO_3 and BO_4 units vary (Hassib et al. 2019). Various factors need to be taken into account when selecting which metal oxides to add to the glasses. These include the oxides' mechanical, thermal, optical, and, of course, radiation shielding capabilities. Adding bismuth oxide to borate glasses allows them to exhibit outstanding infrared transmission as well as non-linear optical characteristics, which attracts the attention of many researchers. However, bismuth oxide alone cannot form a glass network due to its limited field strength. Bismuth oxide-containing glasses find use in thermal and mechanical sensors, opto-electronic device layers, glass ceramics, and reflecting windows (Kaky et al. 2017, 2020).

Transition metal-doped glasses have received greater attention than other glass materials because of their special properties; these include their level of sensitivity to nearby cations, their partially occupied d-shell with extremely reactive electrons, and their distinctive features resulting from the existence of transition metal ions across several valence states inside the glass matrix (Marzouk et al. 2016; Morshidy et al. 2022; Abul-magd et al. 2022; Hameed et al. 2021; Srinivas et al. 2022). The energy levels (d–d transitions) produced by the TM ions implanted in the host glass frameworks will be distinct. These dopants can improve the glasses' useful applications by serving as probes to find such changes in energy levels.

Titanium oxide glasses, one of the many types of transition metal oxide-doped glasses, have attracted attention lately because of their possible use in non-linear optical systems, such as power limiters and ultrafast switches. Titanium oxide is commonly considered a crystal nucleating agent through silicate glasses. All other glass matrices, on the other hand, have been demonstrated to contain trace levels of TiO_2, which enhances the glasses' ability to form glass and their resilience to chemicals. It is acknowledged that there are two valence states for titanium ions in glasses: the tetravalent (Ti^{4+}) and the trivalent (Ti^{3+}) forms (Khattari et al. 2022a; Rammah et al. 2022). Glass composition and type, as well as melting conditions, determine the ratio of each state in the glass. The vacant or unfilled d-shells of Ti^{4+} ions play a more significant role in the non-linear polarizabilities. Numerous optical applications, including optical signal processing, optical computers, and a lot more, rely heavily on nonlinear optics. Furthermore, since the presence of these ions in a glass network may dramatically change a wide range of physical characteristics, including color, chemical resistivity, tensile strength, and insulating qualities (Raoa et al. 2005). Another interesting property of this material is the Ti–O bond length (~ 1.96 Å), which can greatly boost the non-linear polarizabilities of TiO_2 (Alajerami et al. 2013). TiO_2 is a glass-forming agent that promotes a more polymerized structure and increases the glass's stability against devitrification. The development of glasses with low tanδ and high ε' values enhances their potential for energy storage applications.

Examining the effects of titanium ions on the structural, dielectric, and radiation properties of bismuth-zinc-borate glasses is the principal objective of this work.

2 Experimental

2.1 Synthesization of glasses

Glass blocks (65 − x) B_2O_3–5Bi_2O_3–15ZnO–15BaO–xTiO_2 were made using the conventional melt quenching method with x ranging from 0.0 to 10 with 2.0 mol% increments. Bi_2O_3, ZnO, BaO, TiO_2, and B_2O_3 were the 99% pure raw ingredients that were employed. Each composite has a produced weight of 12 g total. The weighed powders in accordance with the molar ratio (refer to Table 1) are combined in a mortar for thirty minutes to produce an excellent, homogenous mixture. The resultant mixtures were then put into 50 mL uncoated ceramic pots and heated at 300 °C for 50 min. After that, it was moved to a second electrical oven and cooked at 1200 °C for 40 min, yielding a clear, very viscous liquid. The glass liquid was put into an iron cylinder to make samples. The finished glasses were subsequently baked at 300 °C for three hours in a muffled oven. In order to prepare the created glasses for the next measurements, they were polished.

2.2 Physical measurements

The density of the generated glass samples was calculated in a laboratory setting utilizing the Archimedes Principle and the following formula:

$$\rho_{glass} = \frac{W_{Air}}{\left(W_{Air} - W_{Liquid}\right)} \times \rho_{Liquid} \quad (1)$$

The weights of the sample in liquid and vacuum are denoted by W_{Liquid} and W_{Air}, respectively.

JASCO, FT/IR-430 spectrometer (Japan) was utilised to conduct FTIR measurements within the 4000–400 cm^{-1} range.

Table 1 Sample codes, chemical composition, density and molar volume of the prepared Ti-X glasses

Sample code	Glass composition	Density (g/cm^3)
Ti-0.0	65B_2O_3–5Bi_2O_3–15ZnO–15BaO	3.70
Ti-2.0	63B_2O_3–5Bi_2O_3–15ZnO–15BaO–2Ti_2O	3.77
Ti-4.0	61B_2O_3–5Bi_2O_3–15ZnO–15BaO–4Ti_2O	3.81
Ti-6.0	59B_2O_3–5Bi_2O_3–15ZnO–15BaO–6Ti_2O	3.84
Ti-8.0	57B_2O_3–5Bi_2O_3–15ZnO–15BaO–8Ti_2O	3.88
Ti-10.0	55B_2O_3–5Bi_2O_3–15ZnO–15BaO–10Ti_2O	3.93

2.3 Dielectric spectroscopy

The dielectric property elements of the produced glasses have been analyzed using the HIOKI 3532-50 LCR Hi-tester device, which runs in the frequency range of 50 Hz to 5 MHz with a fixed supply voltage of 1 V. The 1 cm-radius circle employed in the study was softened and painted with silver on both faces before it was positioned between two electrodes and applied the same amount of spring tension in the testing cell. The examined glasses' capacitances (C) and resistances (R) were measured 14 times at all selected frequencies, and LabVIEW-based software was used to determine the mean value. The following formulas (Farha et al. 2024; Elsad et al. 2023, 2021) can be used to compute loss tangent (tan δ) and dielectric constant (ε′):

$$\varepsilon' = \frac{tC}{\varepsilon_o A} \tag{2}$$

$$\tan\delta = \frac{1}{2\pi fRC} \tag{3}$$

where sample thickness, tiny electrode cross-section area, applied field frequency, and free space permittivity are represented by the letters t, A, and f, respectively.

2.4 γ-ray buildup factors

The mathematical background and models employed to evaluate the γ-ray buildup factors for the studied glasses, readers can refer to Refs. (Şakar et al. 2020; Naseer et al. 2021; Divina et al. 2020; American National Standard 1991; Ferrari 2005) and the Supplementary materials included with this article.

2.5 Neutron fast neutron removal cross-section (FCS)

The glass samples' medium's fast neutron removal cross-section (FCS) is a typical way to describe its neutron-slowing properties. The linear attenuation coefficient defines the interaction between photons and matter; the removal of fast neutrons by materials can be seen as an analog of this (FCS, cm^{-1}). Also, the following formulas were used to find the half value layer (HVL_{FCS}) and relaxation length (λ_{FCS}) according to the neutrons calculations for the materials. The relaxation length is the mean distance that a fast neutron can move before it interacts with the medium (Maksoud et al. 2022; Kassem et al. 2023):

$$HVL_{FCS} = \frac{\ln 2}{FCS} \tag{4}$$

$$\lambda_{FCS} = \frac{1}{FCS} \tag{5}$$

3 Result and discussion

3.1 Density

The densities of glasses doped with different amounts of titanium oxide are shown in Table 1. When the quantity of titanium rose from 0 to 10 mol%, the density for these glasses increased slightly, from 3.70 to 3.93 g/cm^3. This density gain is caused by a high titanium oxide density (4.23 g/cm^3) compared to the more lightweight borate element (2.46 g/cm^3). Another factor contributing to the greater density of the glasses under investigation is the dopant titanium oxide's higher molecular weight (79.86 g/mol) compared to B_2O_3 (69.617 g/mol).

3.2 FT-IR characterization

FT-IR spectra for the generated glass samples have been analyzed to illustrate the different peaks that characterize the different supposed metal oxide forms in the glass samples. The FT-IR spectra for all the glass samples established the main structure of the glass sample before and after doping with different percentages of Ti^{+2} as shown in Fig. 1 and Table 2. The main peaks of the FT-IR spectra for the glass system (65 − x) B_2O_3–5Bi_2O_3–15ZnO–15BaO–xTiO_2 for the following TiO_2 doping percentages 0%, 2%, 4%, and 6% were observed as the following: the main characteristic peaks for ZnO appeared around 450, and 540 cm^{-1} referring to bond vibrations of Zn–O in its tetrahedral form ZnO_4 (He et al. 2014). The peaks for B_2O_3 appeared at around 735, 1295, and 1450 cm^{-1}, due to B–O bond vibrations in BO_3 in its trigonal form. The borate

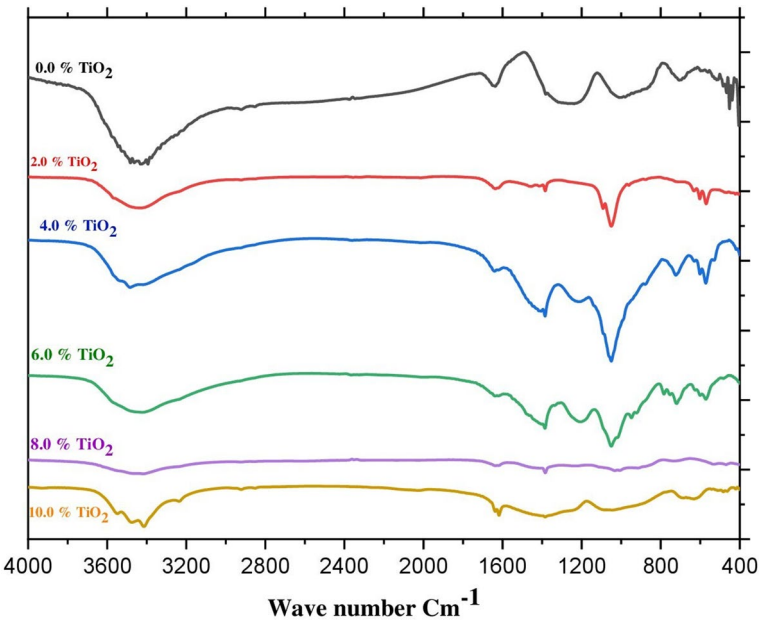

Fig. 1 FTIR spectra of prepared glasses doped with titanium oxide: [(65 − x) B_2O_3–5Bi_2O_3–15ZnO–15BaO–xTiO_2 with x = 0.0, 2.0, 4.0, 6.0, 8.0, and 10.0 mol%]

Table 2 A summary of FT-IR spectra at different band positions of the prepared Ti-X glasses

No	Wave number cm^{-1}	Functional group
1	400–500	Ti–O–Ti vibrations
2	450, and 540	Bond vibrations of Zn–O in its tetrahedral form ZnO_4
3	735, 1295, and 1450	B–O bond vibrations in BO_3 in its trigonal form
4	520	Bi–O stretching vibrations that distorted BiO_6 in its octahedral units
5	500, 740, and 865	Bi–O bond in its BiO_6 form, or the Bi–O bond in BiO_3
6	735	Bi–O bond's symmetric stretching vibrations in its pyramidal BiO_3 form
7	740	B–O–B bending in its borate network
8	200–800	stretching of the B–O bond in its tetrahedral BO_4 form
9	900	Bi–O bonds symmetric stretching vibrations in pyramidal BiO_3 form, Or B–O bonds stretching vibrations in the BO_4 form
10	1050	B–O stretching vibrations in tri borates B_3O_5, tetra borate B_8O_{132}–, and Penta borate B_5O_8–
11	1100	B–O bonds stretching vibrations in BO_3 form due to the presence of meta, and ortho borate
12	1295	B–O bonds asymmetrical stretching vibrations in BO_3 form
13	1200–1600	B–O bonds asymmetric stretching in BO_3 form

glass vibrations generally occur in three infrared areas. The first one, which spans 1200–1600 cm^{-1}, is caused by the B–O bonds in the BO_3 form stretching asymmetrically. The B–O bond stretching in its tetrahedral BO_4 form was described in the second range, which was between 800 and 200 cm^{-1}, and the B–O–B bending in its borate network was described in the third group, which was about 740 cm^{-1} (He et al. 2014; Iordanova et al. 1996). The peak around 1050 cm^{-1} referred to B–O stretching vibrations in tri borates B_3O_5, tetra borate $B_8O_{13}{}^{2-}$, and Penta borate $B_5O_8{}^{-}$. The peak around 1100 cm^{-1} referred to B–O bonds stretching vibrations in BO_3 form due to the presence of meta, and ortho borate. The broad peak around 1295 cm^{-1} referred to the B–O bonds asymmetrical stretching vibrations in BO_3 form (He et al. 2014; Iordanova et al. 1996). The main characteristic peaks for Bi_2O_3 appeared around 520 cm^{-1} due to the Bi–O stretching vibrations that distorted BiO_6 in its octahedral units. Also, this peak may overlap with B–O–B bond-bending vibrations (He et al. 2014; Kamitsos et al. 1989). The peak is around 735 cm^{-1} due to the Bi–O bond's symmetric stretching vibrations in its pyramidal BiO_3 form. The peak around 900 cm^{-1} referred to Bi–O bonds symmetric stretching vibrations in pyramidal BiO_3 form, also this peak may be interfered with B–O bonds stretching vibrations in the BO_4 form (He et al. 2014; Kamitsos et al. 1989). Also, the peaks around 500, 740, and 865 cm^{-1} may be referred to as the Bi–O bond in its BiO_6 form, or referred to as the Bi–O bond in BiO_3 (He et al. 2014; Kamitsos et al. 1989). In case the two-glass system doped with 8, and 10% of TiO_2 most of the previously mentioned peaks intensity decreased and this is an indication of the formation of new bonding through the Ti^{+2}, in the glass containing TiO_2.The peaks that appeared between 400 and 500 cm^{-1} referred to Ti–O–Ti vibrations, as well as the Ti–O vibrations. In these two systems, there is a shift in the peak's position and the intensity of the peaks decreases by increasing the percent TiO_2 in the synthesized glass samples (Kumar et al. 2021).

3.3 Dielectric spectroscopy

Figure 2 displays the frequency dependence of ε′ for (65 − x) B_2O_3–5Bi_2O_3–15ZnO–15BaO–xTiO_2. It is clear that for all samples, ε′ falls with increasing frequency, which is consistent with oxide glasses' typical behavior (Alsaif et al. 2022b, 2023c; Habashy et al. 2021; Abdel-Aziz et al. 2022; Elsad et al. 2019). Dipolar as well as space charge polarizations are the causes of the low-frequency value of ε′ (Abdel-Aziz et al. 2022). The permanent dipoles along the specimen are oriented in the direction of the supplied electric field, which results in dipolar polarization. On the other hand, the polarization of space charges results from the build-up of mobile carrier charges at interfaces. Furthermore, the material's amorphous nature is revealed by the high value of ε′, which denotes the impact of conductive ionic mobility and space charge polarization (Abdel-Aziz et al. 2022; Elsad et al. 2019; Alsaif et al. 2023c; Shams et al. 2021). The dipolar, as well as space charge polarizations, steadily lessen as frequency rises, which causes the value of ε′ to decrease until it reaches an unchanged level at high frequencies. As a result, when the frequency of the field applied is increased, the dipoles have less time to rotate quickly and are unable to follow the line of the applied field (Abdel-Aziz et al. 2022; Alsaif et al. 2023c).

The dependence of the dielectric constant (ε′) on titanium loading at a frequency of 3 kHz is depicted in Fig. 3. According to this figure, the ε′ value is semi-constant up to 4 weight percent of titanium doping and noticeably rises with additional doping. The degree of produced interconnectivity across all glass structure ingredients has a significant impact on the dielectric constant (Alsaif et al. 2022b; Shams et al. 2021; Ali et al. 2020). Because of titanium oxidation, there are more charge carriers when the concentration of titanium increases. The semi-constant ε′, which was observed during the titanium doping process from 0.0 to 4 weight percent, represents the equilibrium between the increase in charge

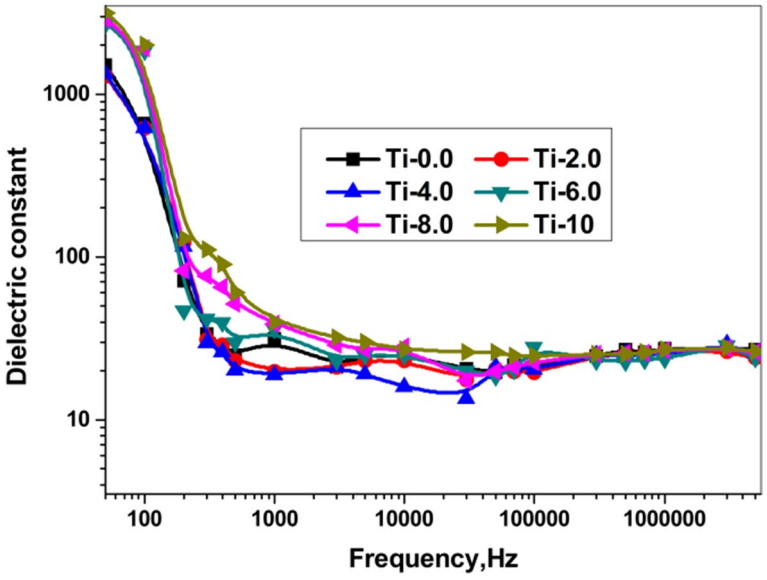

Fig. 2 dependence dielectric constant on the applied frequency at RT for prepared glasses doped with titanium oxide: [(65 − x) B_2O_3–5Bi_2O_3–15ZnO–15BaO–xTiO_2 with x = 0.0, 2.0, 4.0, 6.0, 8.0, and 10.0 mol%]

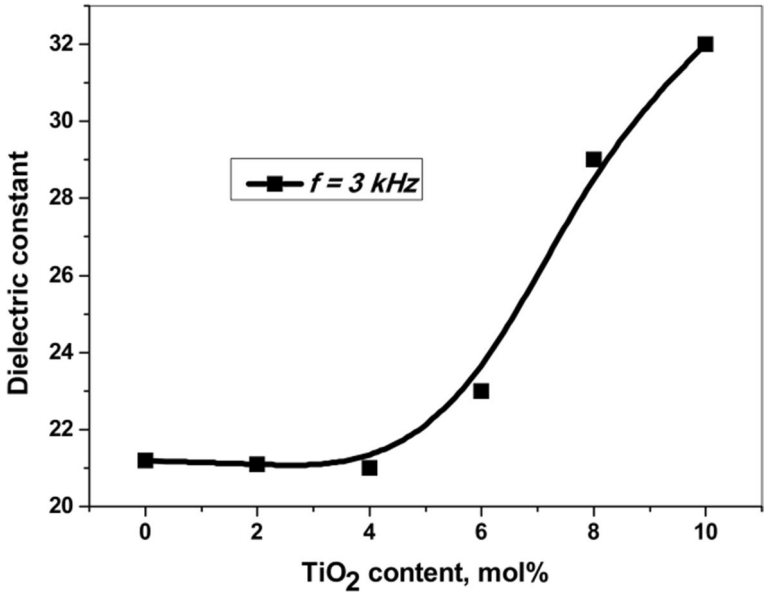

Fig. 3 Variation of dielectric constant (ε′) with titanium content at RT

carriers and the improvement in interconnectivity across all glass structure constituents. The high dose of titanium alters the glasses' structure by rupturing the B–O–B bond, which increases the flexibility of charge carriers that form up at interfaces and increases the polarization of space charge. More precisely, as titanium concentration rises, more charge carriers are present, and the production of trivalent (Ti^{3+}) and tetravalent (Ti^{4+}) couples correspondingly quickens. Thus, the dielectric constant rises in tandem with the polarization of charges (ElBatal et al. 2016).

Figure 4 illustrates the dissipation factor, tan δ, for (65 − x) B_2O_3–$5Bi_2O_3$–15ZnO–15BaO–xTiO_2. As shown in the figure, the tan δ across glasses doped with different amounts of titanium decreased in the lower frequency zone of the utilized field and stabilized in the higher frequencies sector with the establishment of some interfacial relaxing. In fact, there is a close relationship between electrical conductivity and the tan δ value (Alsaif et al. 2023c; Shams et al. 2021; Ali et al. 2020). Tan δ reduced substantially in the low-frequency zone because there was considerably less free charge carrier hopping since there was not a sufficient amount of time for an outside electric field to reverse. The dielectric relaxing at low frequency could perhaps be attributed to the interfacial polarization process (Elsad et al. 2019; Alsaif et al. 2023c; Shams et al. 2021; Ali et al. 2020; Mansour et al. 2016).

3.4 γ-ray buildup factors

Figures 5 and 6 show the exposure (EBF) and energy absorption (EABF) buildup factors values as a function of photon energy for the substances studied at 1–40 MFP. Sample composition, penetration depth, and photon energy all have an impact on the BUF's upper limits. At deeper depths, several scatterings take place. The BUFs readings were highest at

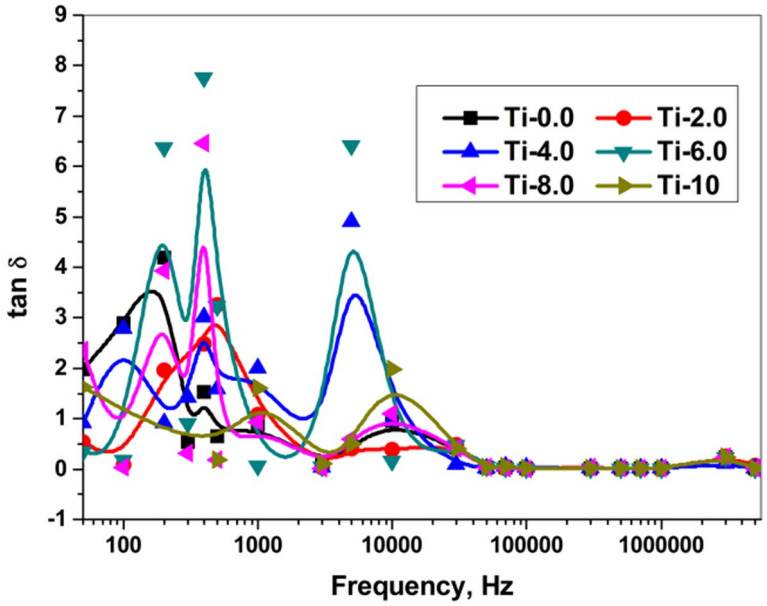

Fig. 4 Variation of tan δ with the applied frequency at RT for prepared glasses doped with titanium oxide: $[(65 - x)\ B_2O_3–5Bi_2O_3–15ZnO–15BaO–xTiO_2$ with x = 0.0, 2.0, 4.0, 6.0, 8.0, and 10.0 mol%]

40 MFPs, and lowest at 1 MFPs. As seen in Figs. 5 and 6, the BUF values increase with photon energy up to a maximum, then decrease with further increases in photon energy. Since interactions at low energies are dominated by the photoelectric effect (PEE), a significant amount of photons have been absorbed and the BUFs are lowest (Basu et al. 2021). The largest BUFs values are seen in the intermediate photon energy (Eγ) range because the prevalent Compton scattering (CS), but cannot destroy it. Once more, the photons were absorbed in the larger energy region, where the primary interaction is pair formation (PaP) (Saleh et al. 2022).

3.5 Neutron fast neutron removal cross-section (FCS)

Figure 7 shows the fast neutrons removal cross-section (FCS) for the six prepared Ti-X glass samples which were 0.108, 0.109, 0. 109, 0. 109, 0. 109, and 0.110 cm^{-1}, for Ti-X glasses where X = 0.0, 0.2, 0.4, 0.6, 0.8, and 10.0, respectively. Because of its high density (3.930 g cm^{-3}) and high amount of light components, the Ti-10.0 glass sample, which has the maximum doping of TiO_2, has the most successfully removed cross-section.

In addition, as shown in Fig. 7, the FCS for the ready Ti-X samples were compared to those of three commercial concrete compounds—limonite/sand concrete (BLC), goethite/sand/boron carbides mixed with concrete (BGC), and commercial glass samples, RS-253-G18, RS-360, RS-520, and TZNNd9 (Sabry et al. 2021; Nabil et al. 2023; Abd Elwahab et al. 2019; Khalil et al. 2024; Salem et al. 2023; Zakaly et al. 2023). The Ti-X glass samples' FNRCS value was found to be higher than that of the commercial concrete and glass samples that were tested, and lower than that of the polymer samples. The Ti-X glasses that are being studied are probably superior at shielding against neutrons. Figure 8 also displays the HVL_{FCS} and λ_{FCS}

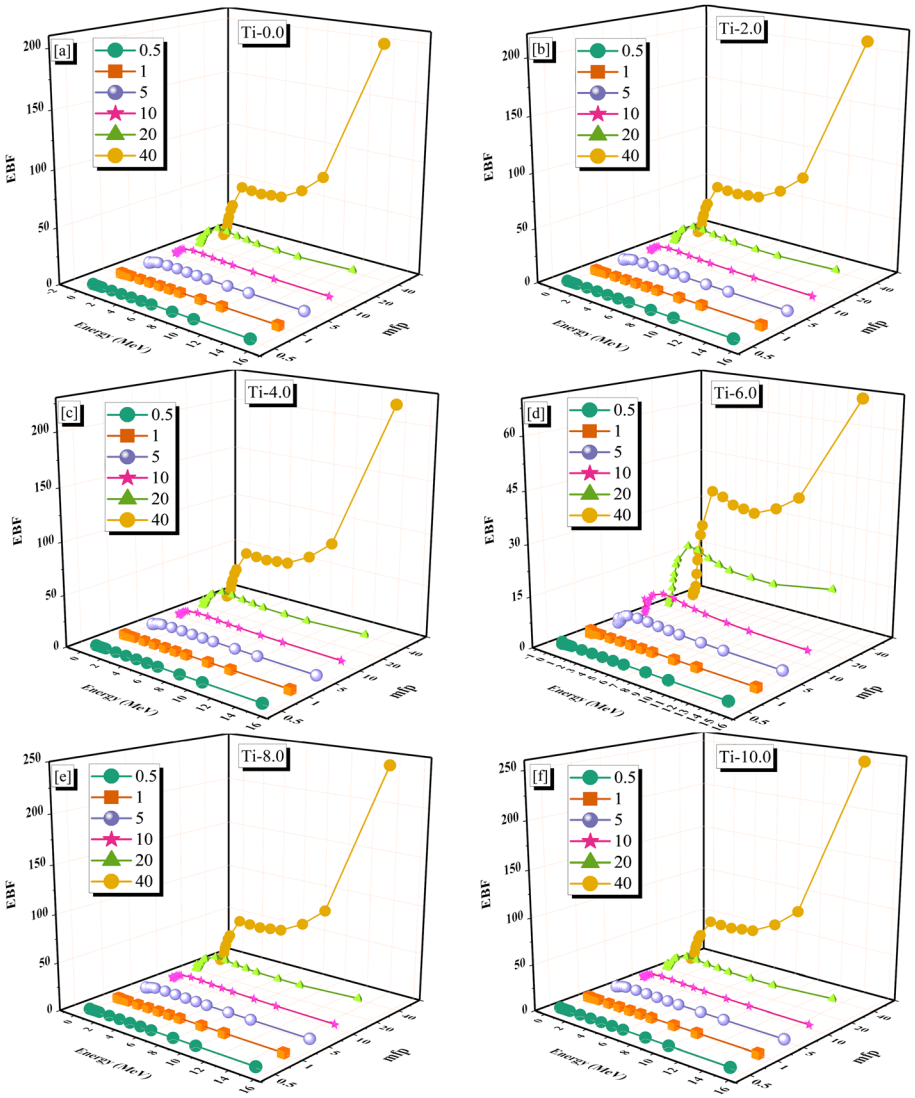

Fig. 5 The exposure buildup factor (EBF) vs. photon energy for the prepared samples **a** Ti-0.0, **b** Ti-2.0, **c** Ti-4.0, **d** Ti-6.0, **e** Ti-8.0, and **f** Ti-10.0

for the prepared Ti-X glass sample. Based on the simulated FCS values, the HVL_{FCS} and λ_{FCS} values were the lowest for the Ti-10.0 glass sample. Better neutron shielding properties are found in Ti-X glasses under investigation.

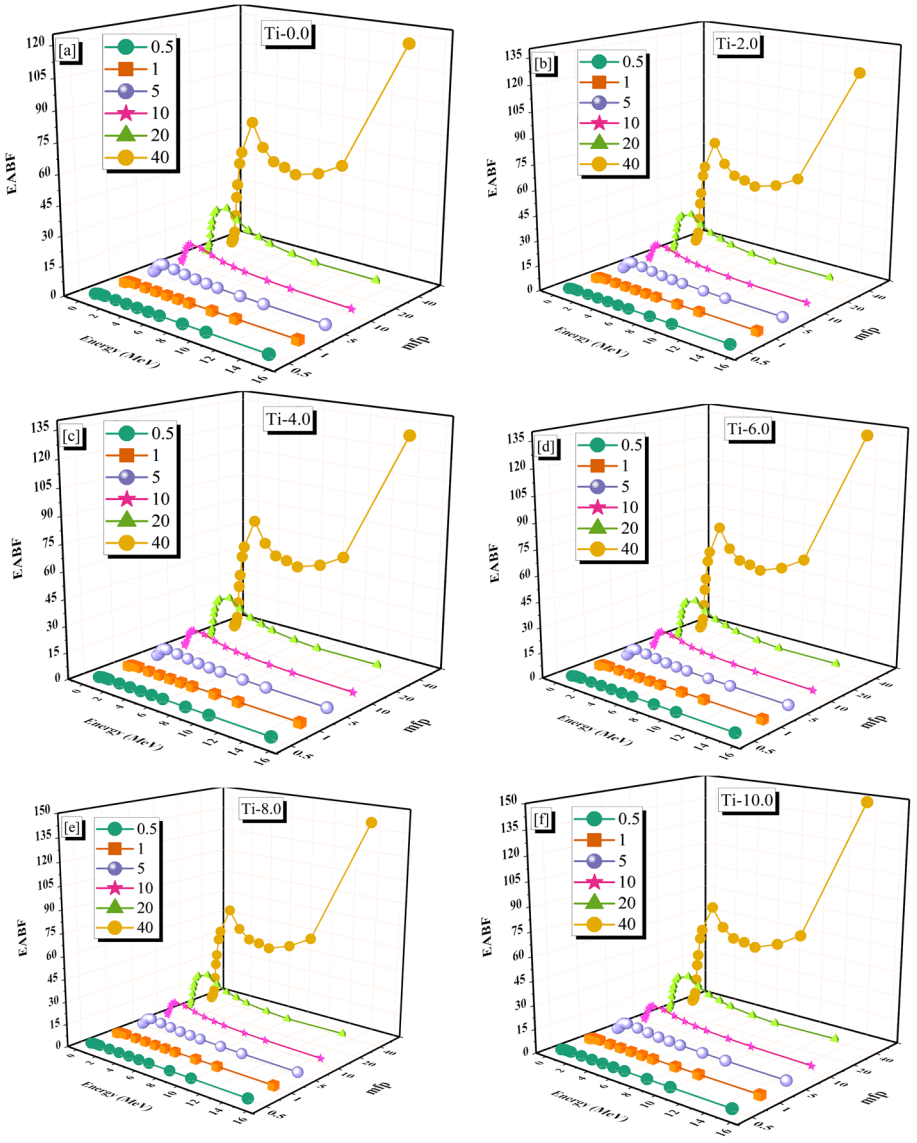

Fig. 6 The energy absorption buildup factor (EABF) vs. photon energy for the prepared glass samples **a** Ti-0.0, **b** Ti-2.0, **c** Ti-4.0, **d** Ti-6.0, **e** Ti-8.0, and **f** Ti-10.0

4 Conclusion

In this work, we experimentally examined the impacts of TiO_2-doping on the structural, shielding, and dielectric spectroscopic modifications of glass blocks: (65 − x) B_2O_3–5Bi_2O_3–15ZnO–15BaO–xTiO_2. According to the findings, the density of the suggested glasses somewhat increased when the glassy network's TiO_2 mol% level rose. The studied glasses treated with TiO_2 up to 4 mol% exhibited a stable dielectric constant;

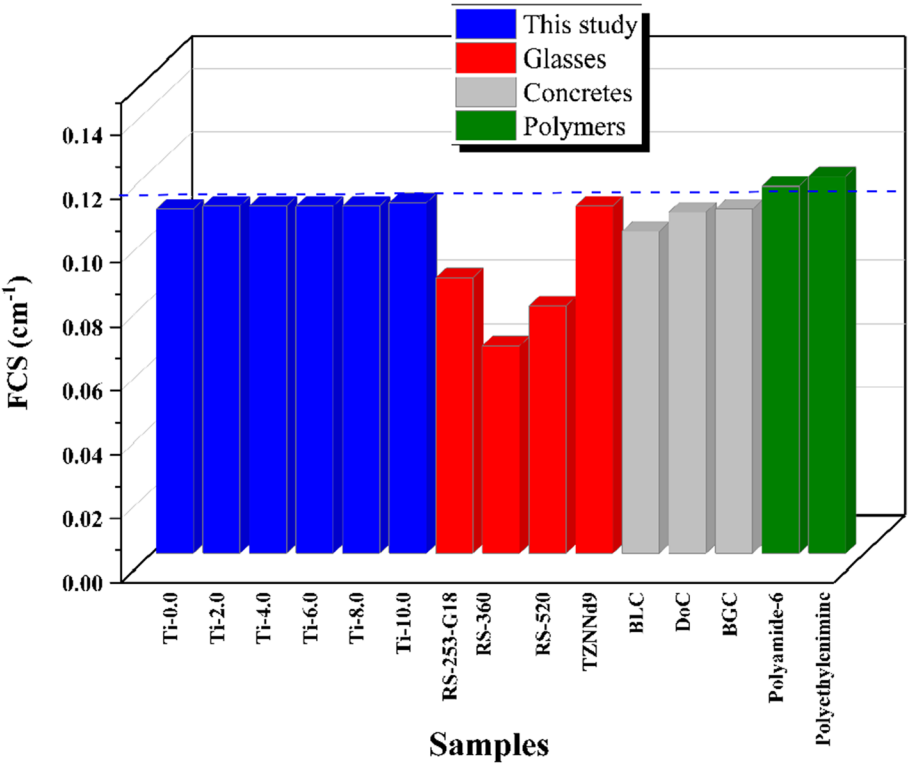

Fig. 7 Comparison of The fast neutron removal cross-section (FCS) for the prepared Ti-X glass samples and commercial glass and concrete samples

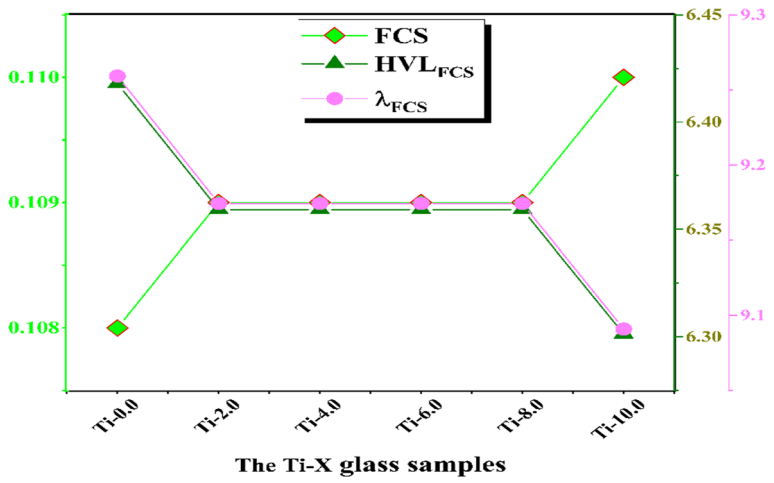

Fig. 8 The fast neutron removal cross-section (FCS), the half value layer (HVL_{FCS}), and the relaxation length (λ_{FCS}) for the prepared Ti-X glass samples

however, their dielectric constant increased with increasing TiO_2 concentration. High-titanium (Ti-10) glass sample is thought to be the best option for energy storage applications. The Phy-X/PSD software was employed to estimate the exposure (EBF) and energy absorption (EABF) buildup factors of Ti-X glasses as a function of photon energy at 1–40 MFP. Both EBF and EABF increased with photon energy up to a maximum, then decline with additional increases in photon energy according to PEE, CS, and PaP interactions. The glass sample Ti-10.0 had the highest removal cross-sectional efficiency. The sample Ti-10.0 had the lowest relaxation length (λ_{FCS}) and half value layer (HVL_{FCS}).

Supplementary Information The online version contains supplementary material available at https://doi.org/10.1007/s11082-024-06809-6.

Acknowledgements This work was funded by the Deanship of Scientific Research at Princess Nourah bint Abdulrahman University, through the Research Groups Program Grant No. (RGP-1444-0055).

Author contribution All authors contributed to conceptualization, methodology, software, validation, investigation, data curation, writing—review and editing, and visualization.

Funding Deanship of Scientific Research, Princess Nourah Bint Abdulrahman University, RGP-1444-0055.

Data availability Relevant research data are included in the text of the work.

Declarations

Conflict of interest The authors declare that they have no conflict of interest.

References

AbdElwahab, N.R., Helal, N., Mohamed, T., Shahin, F., Ali, F.M.: New shielding composite paste for mixed fields of fast neutrons and gamma rays. Mater. Chem. Phys. **233**, 249–253 (2019)

Abdel-Aziz, A.M., Elsad, R.A., Ahmed, E.M., Rammah, Y.S., Shams, M.S., Misbah, M.H.: Synthesis, physical, ultrasonic waves, mechanical, FTIR, and dielectric characteristics of $B_2O_3/Li_2O/ZnO$ glasses doped with Y^{3+} ions. J. Mater. Sci. Mater. Electron. **33**, 6603–6615 (2022)

Abul-magd, A.A., Basry, A.A.H., Abu, S.M., Hassan, E., Abu-khadra, A.S.: Interplay between structural modifications and optical/luminescence response in Mn-doped alkali borate glasses. Mater. Chem. Phys. **288**, 126381 (2022)

Alajerami, Y.S.M., Hashim, S., Ghoshal, S.K., Saleh, M.A., Kadni, T., Saripan, M.I., Alzimami, K., Ibrahim, Z., Bradley, D.A.: The effect of TiO_2 and MgO on the thermoluminescence properties of a lithium potassium borate glass system. J. Phys. Chem. Solids **74**, 1816–1822 (2013)

Ali, S.F.A., Elsad, R.A., Mansour, S.A.: Enhancing the dielectric properties of compatibilized high-density polyethylene/calcium carbonate nanocomposites using high-density polyethylene-g-maleic anhydride. Polym. Bull.. Bull. **10**, 1–13 (2020)

Alrowaili, Z.A., Khattari, Z.Y., Alsaif, N.A., Shams, M.S., El-Refaey, A.M., Elsad, R.A., Al-Buriahi, M.S., Rammah, Y.S.: Synthesis, physical properties, neutron, and gamma-ray shielding competence of borate-based glasses reinforced with erbium (III) oxide: a closer-look on the impact of Eu_2O_3. J. Mater. Sci. Mater. Electron. **34**, 221 (2023)

Alsaif, N.A.M., Elsad, R.A., Sadeq, M.S., Rammah, Y.S., Ahmed, E.M., El-Hamalawy, A.A., Shams, M.S.: Antimony (III) oxide-reinforced lithium-calcium borate glasses: preparation and characterization of physical, optical, and γ-ray shielding behavior through experimental and theoretical methods. J. Electron. Mater. **51**, 5869–5879 (2022a)

Alsaif, N.A.M., Khattari, Z.Y., Rammah, Y.S., Shams, M.S., Elsad, R.A.: Bismo-borate glasses doped with La^{3+} and Eu^{3+} ions: synthesis, physical, optical and electrical characteristics. J. Mater. Sci. Mater. Electron. **33**, 19667–19677 (2022b)

Alsaif, N.A.M., Ahmmad, S.K., Khattari, Z.Y., Abdelghany, A.M., El-Refaey, A.M., Rammah, Y.S., Shams, M.S., Elsad, R.A.: Synthesis, structure, radiation attenuation efficacy as well as prediction

of density using artificial intelligence techniques of lead borate lithium zinc strontium glasses. Opt. Mater. **137**, 113599 (2023a)
Alsaif, N.A.M., Khattari, Z.Y., Shams, M.S., Rammah, Y.S., El-Refaey, A.M., Elsad, R.A.: Elastic-mechanical, dielectric properties, and γ-radiation safety competence of calcium boro-zinc glass systems reinforced with Nb^{5+} ions: experimental and theoretical studies. J. Mater. Sci. Mater. Electron. **34**, 402 (2023b)
Alsaif, N.A.M., Shams, M.S., El-Refaey, A.M., Rammah, Y.S., Chaurasia, M.A., Siddiqui, N., Elsad, R.A., Ahmmad, S.K.: On cobalt zinc boro sodium fluoride glasses doped with Y_2O_3: synthesis, artificial intelligence density prediction and dielectric spectroscopy. Optik **281**, 170849 (2023c)
American National Standard.: Gamma-ray attenuation coefficients and buildup factors for engineering materials, ANSI/ANS-6.4.3 (1991)
Basu, P., Sarangapani, R., Venkatraman, B.: An improvement to the Kalos' formula for double layer gamma ray exposure buildup factors for shielding materials of nuclear and radiological facilities. Ann. Nucl. EnergyNucl. Energy **151**, 107944 (2021)
Divina, R., Naseer, K.A., Marimuthu, K., Alajerami, Y.S.M., Al-Buriahi, M.S.: Effect of different modifier oxides on the synthesis, structural, optical, and gamma/beta shielding properties of bismuth lead borate glasses doped with europium. J. Mater. Sci. Mater. Electron. **31**, 21486–21501 (2020)
ElBatal, F.H., Marzou, M.A., ElBatal, H.A.: Optical and crystallization studies of titanium dioxide doped sodium and potassium silicate glasses. J. Mol. Struct.Struct. **1121**, 54–59 (2016)
Elsad, R.A., Mansour, S.A., Izzularab, M.A.: Loading different sizes of titania nanoparticles into transformer oil: a study on the dielectric behavior. J. Sol-Gel Sci. Technol. **93**, 615–622 (2019)
Elsad, R.A., Mahmoud, K.A., Rammah, Y.S., Abouhaswa, A.S.: Fabrication, structural, optical, and dielectric properties of PVC-PbO nanocomposites, as well as their gamma-ray shielding capability. Radiat. Phys. Chem.. Phys. Chem. **189**, 109753 (2021)
Elsad, R.A., Habashy, M.M., Izzularab, M.A., Abd-Elhady, A.M.: Evaluation of dielectric properties for PVC/SiO_2 nanocomposites under the effect of water absorption. J. Mater. Sci. Mater. Electron. **34**, 786 (2023)
Farha, A.H., Shams, M.S., Alali, H.A., Alhashem, Z.H., Mansour, S.A., Aleithan, S.H., Elsad, R.A.: Dielectric and thermal behavior investigation of Mn–Zn nano ferrite-fluid for transformer oil applications. Arab. J. Chem. **17**, 105459 (2024)
Ferrari, A., et al.: FLUKA: a multi-particle transport code (Program version 2005), Cern—2005-010 (2005). https://doi.org/10.5170/cern-2005-010
Habashy, M.M., Abd-Elhady, A.M., Elsad, R.A., Izzularab, M.A.: Performance of PVC/SiO_2 nanocomposites under thermal ageing. Appl. Nanosci.Nanosci. **11**, 2143–2151 (2021)
Hameed, A., Balakrishna, A., Srinivas, B., Chandrasekhar, M., Shareefuddin, M., Chary, M.N.: Influence of manganese ions on physical and spectroscopic properties of mixed alkali-alkaline earth oxide borate glasses. Optik **246**, 167810 (2021)
Hassib, M.D., Kaky, K.M., Kumar, A., Şakar, E., Sayyed, M.I., Baki, S.O., Mahdi, M.A.: Boro-silicate glasses co-doped Er^{+3}/Yb^{+3} for optical amplifier and gamma radiation shielding applications. Phys. B Condens. **567**, 37–44 (2019)
He, F., He, Z.J., Xie, J.L., Li, Y.H.: IR and Raman spectra properties of Bi_2O_3–ZnO–B_2O_3–BaO quaternary glass system. Am. J. Anal. Chem. **5**, 1142–1150 (2014)
Iordanova, R., Dimitriev, Y., Dimitrov, V., Kassabov, S., Klissurski, D.: Glass formation and structure in the V_2O_5–Bi_2O_3–Fe_2O_3 glasses. J. Non-Cryst. SolidsCryst. Solids **204**, 141–150 (1996)
Kaky, K.M., Lakshminarayana, G., Baki, S.O., Halimah, M.K., Mahdi, M.A.: Structural thermal and optical studies of bismuth doped multicomponent tellurite glass. Solid State Phenom. **268**, 165–171 (2017)
Kaky, K.M., Şakar, E., Akbaba, U., Kasapoğlu, A.E., Sayyed, M.I., Gür, E., Baki, S.O., Mahdi, M.A.: X-ray photoelectron spectroscopy (XPS) and gamma-ray shielding investigation of boro-silicate glasses contained alkali/alkaline modifier. Results Phys. **14**, 102438 (2019)
Kaky, K.M., Sayyed, M.I., Khammas, A., Kumar, A., Şakar, E., Abdalsalam, A.H., Şakar, B.C., Alim, B., Mhareb, M.H.A.: Theoretical and experimental validation gamma shielding properties of B_2O_3–ZnO–MgO–Bi_2O_3 glass system. Mater. Chem. Phys. **242**, 122504 (2020)
Kamitsos, E.I., Karakassides, M.A., Patsis, A.P.: Spectroscopic study of carbonate retention in high-basicity borate glasses. J. Non-Cryst. SolidsCryst. Solids **111**, 252–262 (1989)
Kassem, S.M., Abdel Maksoud, M., El Sayed, A.M., Ebraheem, S., Helal, A., Ebaid, Y.: Optical and radiation shielding properties of PVC/$BiVO_4$ nanocomposite. Sci. Rep. **13**, 10964 (2023)
Khalil, A., Bondouk, I.I., Allam, E.A., Nabil, I.M., Al-Abyad, M., Saudi, H., El-Taher, A., Mahmoud, M.E., Amar, A.: A binary composite material of nano polyaniline intercalated with Nano-Fe_2O_3 for

enhancing gamma-radiation-shielding properties: experimental and simulation study. Prog. Nucl. Energy. Nucl. Energy **169**, 105067 (2024)

Khattari, Z.Y., Alsaif, N.A.M., Rammah, Y.S., AbouHussein, E.M., Shams, M.S., Elsad, R.A.: Fabrication, physical, mechanical, and radiation protection properties of bismo-borate glasses containing La^{3+} + Eu^{3+} as additive ions. Radiat. Phys. Chem.. Phys. Chem. **201**, 110454 (2022a)

Khattari, Z.Y., Alsaif, N.A.M., Rammah, Y.S., Shams, M.S., Elsad, R.A.: Physical, elastic-mechanical and radiation shielding properties of antimony borate–lithium in the form B_2O_3–CaO–Li_2O–Sb_2O_3: experimental, theoretical and simulation approaches. Appl. Phys. A **128**(9), 796 (2022b)

Kumar, P.P., Bhogi, A., Kalimi, M.R., Reniguntla, P.S.: Influence of TiO_2 ions on structural properties and AC conductivity of BaO–Bi_2O_3–B_2O_3 glass system. Mater. Today Proc. **38**, 2200–2204 (2021)

Lakshminarayana, G., Sayyed, M.I., Baki, S.O., Lira, A., Dong, M.G., Kaky, K.M., Kityk, I.V., Mahdi, M.A.: Optical absorption and gamma-radiation-shielding parameter studies of Tm^{3+}-doped multicomponent borosilicate glasses. Appl. Phys. A **124**, 378 (2018)

Maksoud, M.A., Kassem, S.M., Sallam, O.: Structural, optical, and radiation shielding features of newly developed $BaZrO_3$/Na_2O–B_2O_3 glass. Ceram. Int. **48**, 30938–30950 (2022)

Mansour, S.A., Elsad, R.A., Izzularab, M.A.: Dielectric investigation of high density polyethylene loaded by ZnO nanoparticles synthesized by sol–gel route. J. Sol-Gel Sci. Technol. **80**(2), 333–341 (2016)

Marzouk, M.A., Abo-Naf, S.M., Zayed, H.A., Hassan, N.S.: Photoluminescence and semiconducting behavior of Fe Co, Ni and Cu implanted in heavy metal oxide glasses. J. Mater. Res. Technol. **5**, 226–233 (2016)

Morshidy, H.Y., Mohamed, A.R., Abul-Magd, A.A., Hassan, M.A.: Ascendancy of Cr^{3+} on Cr^{6+} valence state and its effect on borate glass environment through CdO doping. Mater. Chem. Phys. **285**, 126128 (2022)

Nabil, I.M., El-Samrah, M.G., Omar, A., Tawfic, A.F., El Sayed, A.F.: Experimental, analytical, and simulation studies of modified concrete mix for radiation shielding in a mixed radiation field. Sci. Rep. **13**, 17637 (2023)

Naseer, K.A., Marimuthu, K., Mahmoud, K.A., Sayyed, M.I.: Impact of Bi_2O_3 modifier concentration on barium–zincborate glasses: physical, structural, elastic, and radiation-shielding properties. Eur. Phys. J. plus **136**, 116 (2021)

Rammah, Y.S., Al-Buriahi, M.S., Sriwunkum, C., Shams, M.S., Yousef, E.S.: Influence of Er^{3+}-doped ions on the linear/nonlinear optical characteristics and radiation shielding features of TeO_2–ZnO–Er_2O_3 glasses. J. Mater. Sci. Mater. Electron. **31**, 21431–21443 (2020)

Rammah, Y.S., Alsaif, N.A.M., Khattari, Z.Y., Shams, M.S., Elsad, R.A., Sadeq, M.S.: Synthesis, physical, FTIR, and optical characteristics of B_2O_3·CaO·ZnO glasses doped with Nb_2O_5 oxide: experimental investigation. J. Mater. Sci. Mater. Electron. **33**, 23749–23760 (2022)

Raoa, P.N., Kanthb, C.L., Raoa, D.K., Veeraiah, N.: Influence of titanium ions on optical properties of AF–PbO–B_2O_3 glasses. J. Quant. Spectrosc. Radiat. Transf.Spectrosc. Radiat. Transf. **95**, 373–386 (2005)

Sabry, N., Zahran, H., Algarni, H., Umar, A., Albargi, H.B., Yahia, I.: Gamma-ray attenuation, fast neutron removal cross-section and build up factor of $Cu_2MnGe[S, Se, Te]_4$ semiconductor compounds: novel approach. Radiat. Phys. Chem.. Phys. Chem. **179**, 109248 (2021)

Şakar, E., Özpolat, Ö.F., Alım, B., Sayyed, M.I., Kurudirek, M.: Phy-X/PSD: development of a user friendly online software for calculation of parameters relevant to radiation shielding and dosimetry. Radiat. Phys. Chem.. Phys. Chem. **166**, 108496 (2020)

Saleh, A., Shalaby, R.M., Abdelhakim, N.A.: Comprehensive study on structure, mechanical and nuclear shielding properties of lead free Sn–Zn–Bi alloys as a powerful radiation and neutron shielding material. Radiat. Phys. Chem.. Phys. Chem. **195**, 110065 (2022)

Salem, M.M., Kenawy, E., Zakaly, H.M.H., Ene, A., Azaam, M.M., Edries, T.B., Zhou, D., Hussein, M.M., Abd El-Hameed, A.S., Nabil, I.M., Darwish, M.A.: Electrospun PVDF/Barium hexaferrite fiber composites for enhanced electromagnetic shielding in the X-band range. Results Phys. **53**, 106975 (2023)

Shams, M.S., Rammah, Y.S., El-Agawany, F.I., Elsad, R.A.: Synthesis, structure, physical, dielectric characteristics, and gamma-ray shielding competences of novel P_2O_5–Li_2O–ZnO–CdO glasses. J. Mater. Sci. Mater. Electron. **32**, 1877–1887 (2021)

Srinivas, B., Bhogi, A., Naresh, P., Chary, M.N., Shareefuddin, M., Alrowaili, Z.A., Mahmoud, Z.M.M., Olarinoye, I.O., Al-Buriahi, M.S.: Fabrication, optical and radiation shielding properties of BaO–TeO_2–B_2O_3–Cr_2O_3 glass system. Optik **258**, 168877 (2022)

Zakaly, H.M., Ene, A., Olarinoye, O.I., Marzouk, S.Y., Abdel-Hafez, S.H., Shams, M.S., Rammah, Y.S.: Investigation of Er^{3+} ions reinforced zinc-phosphate glasses for ionizing radiation shielding applications. Materials **14**, 6769 (2021)

Zakaly, H.M.H., Nabil, I.M., Issa, S.A.M., Almousa, N., Khattari, Z.Y., Rammah, Y.S.: Probing the elasticity and radiation protection potential of neodymium(III) doped zinc and niobium tellurite glasses: an integrated simulated and applied physics perspective. Mater. Today Commun. **37**, 107113 (2023)